ELSEVIER

International Journal of Mass Spectrometry 192 (1999) 425–436

International Journal of Mass Spectrometry

Formation and cascading decay of hollow Ar atoms at a Si surface

N. Stolterfoht[a,*], J.H. Bremer[a], R. Díez Muiño[b]

[a]*Hahn-Meitner Institut Berlin GmbH, Bereich Festkörperphysik, Glienicker Strasse 100, D-14109 Berlin, Germany*
[b]*Materials Science Division, Lawrence Berkeley National Laboratory, Berkeley, CA 94720, USA*

Received 8 February 1999; accepted 14 March 1999

Abstract

Theoretical work was performed to investigate the formation and cascading decay of hollow Ar atoms during the interaction near a surface of Si. To exhibit the static aspect of hollow atom formation below the surface, the density functional theory was applied to evaluate results for electron charge density plots of atomic orbitals. To study the dynamic properties of hollow Ar atoms, a complex cascade model was developed treating the successive filling of the *K*, *L*, and *M* shells via Auger transitions and collisional charge transfer above the surface and in the bulk. Information is provided for the above- and below-surface contributions in previous experiments of Ar^{17+} impact on SiH using high-resolution x-ray spectroscopy. Clear evidence is given that the velocity-dependent filling of the *M* shell plays a significant role. (Int J Mass Spectrom 192 (1999) 425–436)

Keywords: Hollow atoms; Auger transitions; Electron spectroscopy

1. Introduction

In the past decade, extensive work has been devoted to studies of slow and highly charged ions interacting with a surface [1]. That work has been motivated by the search for unique phenomena created by highly charged ions moving with very low velocities [2–13]. When approaching the surface, a slow and highly charged ion can acquire several electrons by resonant charge transfer from the conduction band of the solid. Thus, in front of the surface, a "hollow" atom is produced with many electrons in higher orbitals and empty intermediate shells [6,12]. The hollow atoms may undergo autoionizing transitions where the electron–electron interaction leads to the ejection of an electron and the relaxation of another electron in a Rydberg orbital.

It is known from the classical over-the-barrier picture that resonant charge transfer takes place into orbitals whose outer boundary just touches the surface. Within the framework of the over-the-barrier model [7] it is assumed that the transfer of the electrons is rapid and that the ion is essentially neutralized in the higher orbitals. Furthermore, the generally accepted scenario implies that lower lying orbitals are continuously filled, and higher lying orbitals are depopulated as the ion approaches the surface [7,13]. Electrons in higher lying orbitals are removed by ejection into the continuum and, more probably, by reentering into the solid. Hence, the

* Corresponding author. E-mail: stolterfoht@hmi.de

1387-3806/99/$20.00
PII S1387-3806(99)00106-2

diameter of the hollow atom gradually shrinks as it approaches the surface.

When the projectile hits the solid, the remaining Rydberg electrons are scattered by the target atoms and are partially removed (peeled off) from the projectile [6,7,13,14]. Simultaneously, during its passage into the surface, the highly charged ion induces a negative charge cloud that is composed of localized continuum orbitals, denoted C [15–17]. This charge cloud is rather intense as it tends to screen the nucleus. The appearance of this intense charge cloud is an outstanding property of a slow highly charged ion moving below the surface [15,16]. Hollow atoms formed below the surface are significantly smaller than those occurring outside the solid. Although the radii of the C orbitals are relatively small, they leave room for an empty space due to unoccupied inner-shell orbitals so that hollow atoms of the second generation are produced. After formation of the cloud C of continuum electrons in the solid, the inner-shell orbitals of the projectile are successively filled by Auger transitions and collisional charge transfer [16].

In their work, Briand and collaborators [6] used the method of x-ray spectroscopy to study highly charged argon projectiles. This method is suitable for Ar, since second-row atoms have a relatively large fluorescence yield providing sufficiently high x-ray intensities. Alternatively, when using Auger electron spectroscopy, primarily first-row atoms (e.g. N and Ne) have been used [8–11]. It is interesting to note that the x-ray studies have led to conclusions which partially disagree with those drawn from the Auger data. Controversial views exist about the role of electron transfer processes between target and projectile atoms. Apparent features of high-resolution x-ray spectra have been attributed to the change from above- to below-surface emission [18–20]. On the contrary, similar features in the Auger spectra from light ions have been interpreted by velocity-dependent charge-transfer processes induced in binary collisions [16,21–23].

Information about light projectiles has been primarily extracted from detailed cascade models studying the occupation of individual configurations [16,22–24]. For a first-row atom, these configuration models are suitable as the corresponding hollow atom has at most two empty shells, i.e. the K and L shells. However, since hollow Ar has an additional empty shell (M), detailed studies of the filling of argon ions are scarce [25,26]. The studies of Ar were often limited to the evaluation of mean numbers of electrons in the shells under study [27,28]. In particular, the high-resolution x-ray spectra produced by Ar^{17+} ions [6,18–20], which provided important information in the field of hollow atoms, have not as yet been interpreted by cascade models treating individual configurations. The high-resolution x-ray spectra yield information about the number of electrons present in the L shell during the emission of the K x rays. Moreover, the centroid energy of individual x-ray peaks provide data about the average number electrons occupying the M shell [6]. Thus, the high degree of information of the observed spectra represent a challenge for models devoted to the dynamic properties of hollow atoms.

In this work, we present theoretical work concerning the impact of Ar^{17+} on a Si surface. To visualize the electron cloud formed around hollow atoms inside the solid, the density of the induced charge cloud was evaluated in a self-consistent manner within the framework of the density functional theory [29]. As a major task, a complex configuration model was developed to describe the cascading decay of hollow Ar atoms. Methods are discussed to determine numerous model parameters and functions. Finally, predictions of the model are shown to compare well with the x-ray spectra by Briand et al. [18]. We confirm their picture of above- and below-surface emission, however, disagree with respect to collisional charge-exchange processes.

2. Formation of hollow Ar atoms

The formation of the hollow atom below the surface is modeled using the density functional theory (DFT), which permits the evaluation of the screening function utilizing a self-consistent field method. In the analysis, the DFT was applied to the problem of a static charge impurity in jellium formed by free

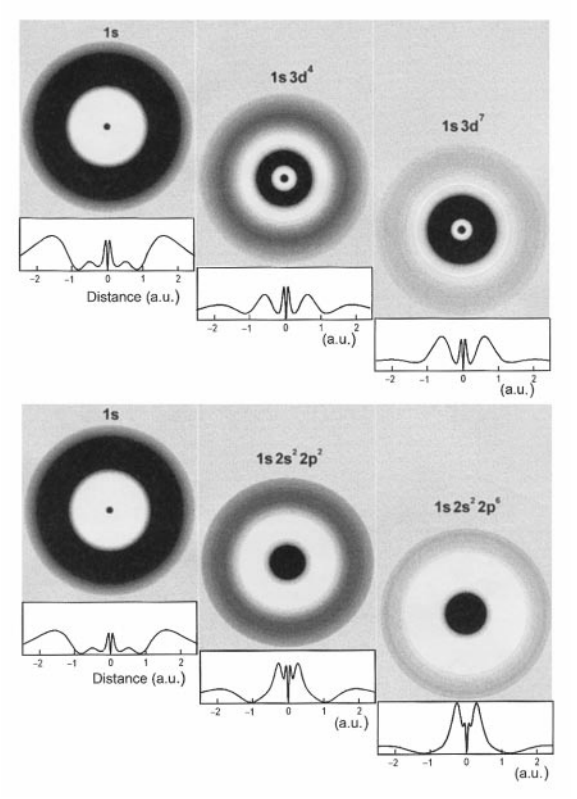

Fig. 1. Electron densities of argon atoms in Si ($r_s = 2$) calculated using the density functional theory [29]. The data are multiplied by $4\pi r^2$ where r is the electronic distance to the argon nucleus. The plot shows two series of graphs which correspond to the filling of the 3d orbital (upper row) and the 2p orbital (lower row).

electrons [29,30]. A value of $r_s = 2$ was chosen that corresponds to an electron density for silicon or aluminum. In particular, we studied highly charged Ar^{q+} ions in Si where q ranges from 9 to 17. Thus, screening functions were determined modeling the features of hollow projectile atoms. More details are given in the previous work by Arnau et al. [15] who have studied the formation of hollow Ne atoms in Al.

To visualize the hollow atom inside the solid, we performed density plots of electronic charge clouds as shown in Fig. 1. At the bottom of the graphs the corresponding density functions are depicted, which were evaluated using the DFT [15,29]. As the hollow atom is neutral, the number of electrons contained in the induced charge cloud is equal to the number of electrons missing in the core. For instance, the hollow atom with one K vacancy and empty L and M shells contains 17 electrons in the induced charge cloud. Below we shall see, however, that this maximum value is only achieved when the inner part of the atom remains empty for a sufficient time.

From the graphs of nearly empty Ar atoms on the left-hand side of Fig. 1, it is seen that the 1s electron density is clearly separated from the induced charge cloud that maximizes near 1.8 a.u. At about 0.8 a.u. the charge density exhibits a deep valley giving rise to a remarkable empty space which is a characteristic feature of the hollow atom. It should be realized that the induced charge density of its maximum is about a factor of 7 more intense than the background density of the conduction band electrons (jellium). This clearly shows the remarkable signature of the hollow atoms formed by a highly charged nucleus, i.e. the large charge cloud induced within the solid. It appears that this feature is more pronounced in the solid as compared to that of the hollow atom located at large distances outside the surface [17].

When the hollow atom moves inside the solid it suffers binary collisions with individual target atoms. In these collisions the upper shells become more and more filled due to charge transfer processes [16]. In addition, Auger processes give rise to a cascadelike filling of the hollow atom. Fig. 1 shows two series of hollow atoms which both start with argon having no electrons in the M and L shell. In the upper series, the 3d orbital becomes occupied with electrons, whereas in the lower series the 2p orbital becomes occupied. As expected, the induced charge cloud around the projectile decreases in intensity as the filling state of the L and M shells increases. Accordingly, as seen from Fig. 1, the empty space diminishes as the hollow atom gets more and more filled in the L and M shell. When 7–8 electrons are located in the Ar atom, the induced charge cloud becomes rather weak.

From the DFT [15,29] we also determined orbital energies for hollow Ar atoms as shown in Fig. 2. It is seen that besides the K and L shells, the M shell involves bound orbitals including the 3d level. For nearly empty hollow Ar the energies of the M shell orbitals are as low as -6 a.u. Furthermore, in a shallow region near the conduction band some bound

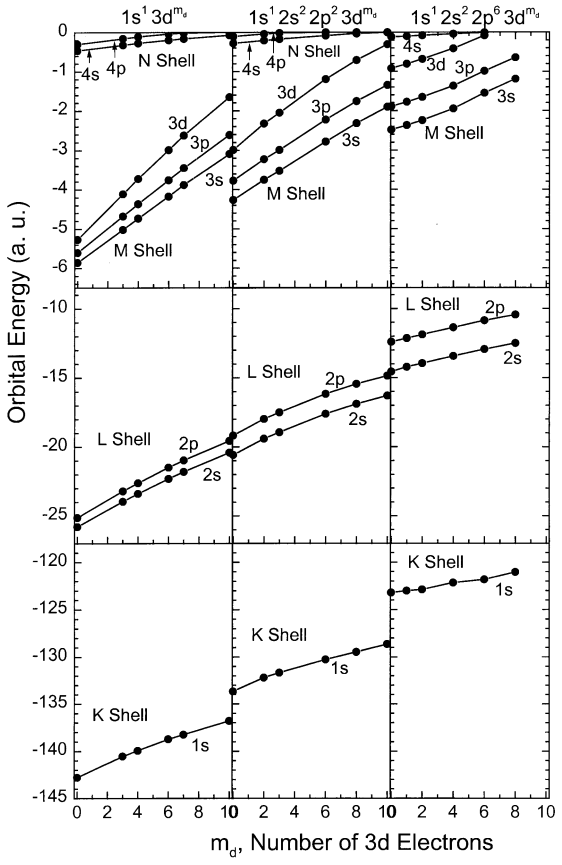

Fig. 2. Orbital energies of hollow, semihollow, and nearly filled Ar atoms in Si as a function of the occupation number m_d of the 3*d* orbital. The energies are obtained by means of the density functional theory [29]. The zero energy corresponds to the bottom of the valence band.

N shell orbitals are visible, too. The shape of the *C* cloud is found to be similar to that of the corresponding atomic *N* shell. Similar phenomena have been observed for the *M* shell in hollow Ne [17]. Thus, when the hollow atom travels through the solid, it is difficult to distinguish the *N* shell from the *C* cloud so that these shells are treated together in the present analysis. Returning to Fig. 2, one notes that the energies of all shells undergo strong variations as an increasing number of electrons are present in the 3*d* orbital of the hollow Ar atom. It should be added that the calculations also provide total energies of the projectile–solid system, which can be used to evaluate Auger transition energies with high precision [15,21].

3. Cascading decay of hollow Ar atoms

3.1. Rate equations

To study the dynamic properties of hollow Ar atoms, a cascade model was developed describing the stepwise filling of their empty inner orbitals near a surface. Although it has some similarities with a previous analysis of Ne [16], the present model includes essentially new developments. Electron transfer processes above the surface are included in the present analysis, whereas the previous model was restricted to below-surface phenomena [16]. The above-surface effects complicate the analysis so that the model equations have to be solved numerically. Moreover, as Ar has an additional shell to be considered, its filling dynamics is significantly more complex than that for Ne. Nevertheless, both cases are governed by sequences that are similar to those known for the radioactive decay of nuclei.

The main task of treating hollow Ar arises from the elaborate bookkeeping of the numerous configurations and decay processes occurring during the stepwise filling of its empty shells. It is recalled from Fig. 1 that the Ar^{17+} ion owns an empty *L* and *M* shell. During the filling of a hollow Ar, the configurations $\kappa = (l, m)$ are transiently produced where *l* and *m* are the numbers of electrons in the *L* and *M* shells, respectively. The transfer from one to another configuration takes place via different radiative and nonradiative electron transitions. Also, collisional electron capture processes into the *M* and the *N* shells are taken into account.

The time evolution of the system is governed by transition rates which are associated with the different electron transfer processes. The Auger transitions are designated by three labels, e.g. the rate $\Gamma_{KLL}(\kappa)$ corresponds to the transfer of an electron from the *L* shell to the *K* shell and also ejecting another *L*-shell electron into the continuum. To keep a consistent notation, two labels are used for x-ray transitions, e.g. $\Gamma_{KL}(\kappa)$, corresponds to the transfer from the *L* shell to the *K* shell (also denoted $K\alpha$ in the literature). The collisional charge transfer is specified by a single label indicating the shell to which the transfer takes

place, e.g. $\Gamma_M(\kappa)$. As noted before, the N shell and higher orbitals, in particular the continuum orbitals, are treated together in one shell labeled C.

An important feature of the model is that the C shell is treated differently from the K, L, and M shells. For the C shell we use the mean-charge method, whereas for the lower shells we apply the configuration method. The mean-charge model is expected to be adequate for the filling of the C shell within the bulk of the solid. To a good approximation, this treatment is also assumed to be valid in the above-surface region where the C shell is used to cover the N shell and higher orbitals. Thus, we consider first the continuous charge parameter q_C which describes the formation of the C shell. The time dependence of q_C is determined by means of the rate equation

$$\frac{dq_C}{dt} = \Gamma_C^{\text{in}}(\kappa, q_C) \tag{1}$$

where Γ_C^{in} is a rate for the charge transfer into the C shell. Within this model, Γ_C^{in} is identified with the rate for resonant charge transfer into the C shell which will be treated in more detail below. At this point we do not consider the transitions from the C shell into lower lying levels as Eq. (1) is solved for fixed configurations $\kappa = (l, m)$. Thus, we obtain a set of functions $q_C(\kappa, t)$ which depend on κ. The fixing of the configurations is released in the following treatment of the L and M shells.

Within the framework of the configuration method, we consider the time-dependent occupation of the configurations κ. To facilitate the task of tracing the system state we use the configuration matrix shown in Fig. 3. Each box in the matrix is associated with a configuration label $\kappa = (l, m)$. The upper level corresponds to ions with a K vacancy, whereas the lower level corresponds to ions with a filled K shell. In the configuration matrix, the stepwise filling of the hollow atom can be traced along sequences of configurations $\{\kappa_1, \kappa_2, \ldots, \kappa_s\}$. The system follows a main configuration sequence, however, there are side paths which have also been included in the present analysis.

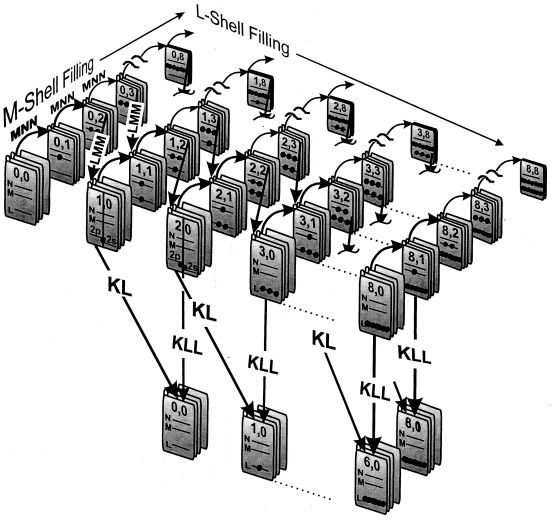

Fig. 3. Configuration matrix used to visualize the filling of hollow Ar atoms. Each box is associated with the configuration $\kappa = (l, m)$ where the labels l and m specify the number of electrons in the L and M shell, respectively. The maximum number of electrons in the M shell is $17 - l$. Radiative and nonradiative transitions are indicated by arrows. Only a few examples of transitions are shown, e.g. the arrows labeled KLL represent Auger transition into the K shell resulting in the emission of an L shell electron. The N shell is treated as part of the C shell, see text. Accordingly, the transitions labeled MNN are referred to as MCC. In a given box the individual folders from the front to the back are associated with an increased filling of the N or C shell.

The Ar^{17+} system starts in the front at the upper-left corner associated with the configuration box (0, 0). The main transition which progresses the system to the (0, 1) box corresponds to an MCC Auger process where an electron from the C shell is transferred into the M shell, and another C electron is ejected. A side path involves an LCC Auger process transferring the system into the (1, 0) box. Furthermore a KLC transition may transfer the system from the (1,0) box into the (0,0) box in the lower level. After sufficient time the system will be distributed over all configuration boxes. At the beginning, the system is centered in the left-front regions at the upper level, whereas with increasing time the system migrates into the right-back region at the lower level.

To visualize individual ingoing and outgoing fluxes consider an arbitrary configuration box (l, m) in the intermediate region of the upper level. The

main ingoing flux is produced by an *MCC* Auger transition from the (l, $m - 1$) box. Likewise, *LMM*, *LMC*, and *LCC* Auger transitions produce flux from the ($l - 1$, $m + 2$), ($l - 1$, $m + 1$), and ($l - 1$, m) boxes, respectively. The outgoing flux involves all possible *MCC*, *LXY*, and *KXY* transitions where *X* and *Y* stand for the *L*, *M*, and *C* shells. Also, radiative *KX* transitions were included, whereas radiative transitions into higher shells (*L*, *M*, etc.) were neglected [31]. It should be added that the steps involving the configurations with $l = 1$ and 2 are processed via the $2p$ and $2s$ subshells (Fig. 3) and the corresponding Coster-Kronig transitions *LLC* were taken into account. The Coster-Kronig transitions are in strong competition with the *K* x-ray transitions, since these radiative dipole transitions into the $1s$ orbital are only possible from the $2p$ level. Finally, single and multiple electron transfer processes into the *M* shell were incorporated by considering binary collisions with target atoms. These transitions provide flux from the boxes (l, $m - i$) where $i = 1, 2, \ldots$.

To calculate the time evolution of the system, we determined the time-dependent occupation number $N_\kappa(t)$ for the configuration κ. Let $\Gamma_i(\kappa)$ and $\Gamma_j(\kappa)$ be the corresponding rates for creation and loss of such configuration, respectively. For a given configuration, multiple paths correspond to several sources of ingoing flux. Similarly, the outgoing flux generally occurs via different paths. Thus, the quantities $N_\kappa(t)$ are obtained by solving the system of rate equations [22,23]

$$\frac{dN_\kappa}{dt} = \sum_i N_{\kappa_i}\Gamma_i(\kappa_i) - N_\kappa \sum_j \Gamma_j(\kappa) \qquad (2)$$

where the labels i and j specify the input and output paths, respectively. This formula shows that the present calculations are elementary, however as mentioned, they require an elaborate selection and bookkeeping of the relevant configurations and transitions.

Some effort is needed to link the mean-charge and configuration methods used in this work. Eq. (2) involves rates associated with the transfer of electrons from the *C* shell. These rates require information about individual electrons occupying the *C* shell. However, information about individual configurations is not achieved when calculating the mean charge from Eq. (1). For instance, when a charge $q_C < 1$ is obtained, it may look like as if, e.g. the radiative *KC* transition is not possible as it requires at least one electron in the *C* shell. However, it should be recalled that q_C stands for a mean value which may involve higher charge states. Hence, to link the mean-charge model with the configuration model, we have to make an assumption about the charge-state distribution associated with a given mean charge. To evaluate the occupation probability P_n of the *C* shell by n electrons we used the binomial distribution formula

$$P_n = \binom{n_{\max}}{n} p^n (1-p)^{n_{\max}-n} \qquad (3)$$

where $n_{\max} = Z - 1 - l - m$ is the maximum number of electrons in the *C* shell and $p = q_C/n_{\max}$. Finally, for the *C* shell in Eq. (2) we used average transition rates that were obtained as a sum of individual rates weighted by the corresponding probability P_n. It is noted that the binomial distribution is important for ions moving above the surface where the *C* shell represents the atomic *N* shell. Below the surface the *C* shell is readily filled with several electrons so that the use of the binomial distribution is not needed.

3.2. Model parameters and functions

The forgoing considerations have shown that the present analysis requires several model parameters and functions whose determination shall briefly be described here. The parameters for x-ray and Auger transitions have either been taken from the literature [31–34] and or evaluated in this work. The values for *KLL* Auger and *KL* x-ray transitions are from Bhalla [32] and Díez Muiño et al. [31] who provided values for all *L*-shell vacancy states. The values were fitted by analytical expressions as shown in Fig. 4. The fits were performed to obtain information about the charge-state dependence of the rates, since in most cases such information is missing. For the *KLL* rates, we used the fit formula

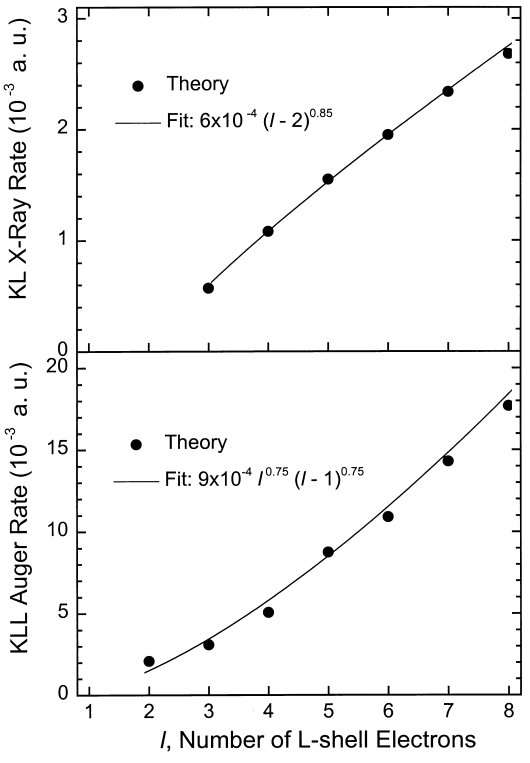

Fig. 4. Calculated rates for *KLL* Auger and *KL* x-ray transitions from [31,32]. The data are fitted by simple formulas, also see text.

$$\Gamma_{KLL}(l) = \Gamma^0_{KLL} l^{\beta}(l-1)^{\beta} \tag{4}$$

where Γ^0_{KLL} is the transition rate per spin state and β is an adjustable parameter. This expression was chosen in accordance with the statistical rule by Larkins [35] who used $\beta = 1$. However, as seen from Fig. 4(b), the fit of the rates [31,32] yields $\beta = 0.75$ in conjunction with $\Gamma^0_{KLL} = 9 \times 10^{-4}$ a.u. Similarly, weaker l-dependencies than proposed by Larkins [35] have previously been used [16,28]. This finding is noteworthy as Larkins' scaling rule is widely applied.

The rates for *KL* x-ray transitions with $l > 2$ (Fig. 4) where fitted by the analytic expression $\Gamma^0_{KL}(l - 2)^{\gamma}$, where Γ^0_{KL} and γ are again adjustable parameters. This procedure takes into account that the radiative rate depend on the number $l_p = l - 2$ of electrons in the $2p$ shell. For $l \leq 2$ the data were kept constant assuming that one electron remains in the $2p$ orbital. The values $\gamma = 0.85$ and $\Gamma^0_{KL} = 6 \times 10^{-4}$ a.u. were obtained by the fit shown in Fig. 4(a). Similarly, the rates for *KM* transition from Bhalla [32] were treated.

To our knowledge *LMM* and *MCC* Auger rates for multiply ionized *L* shell are not available in the literature. These rates were determined under the general assumption that they depend primarily on statistical factors, i.e. the rates per spin state are essentially equal for different shells [28]. In particular, we used the scaling rule

$$\Gamma_{LMM}(l, m) = (8 - l)\Gamma^0_{LMM} m^{\beta}(m-1)^{\beta} \tag{5}$$

which involves the assumption that the rates are proportional to the number of vacancies in the *L* shell. As for *KLL* transitions we set $\beta = 0.75$. The constant $\Gamma^0_{LMM} = 4 \times 10^{-4}$ a.u. was determined by using the known rate for singly charged argon where $l = 7$ and $m = 8$ [27,33]. Similarly, for the *M*–Auger transitions we utilized $\Gamma_{MCC}(m, n) = (18 - m)\Gamma^0_{MCC} n^{\beta}(n-1)^{\beta}$, however, for the *C* shell we assumed a smaller exponent $\beta = 0.5$ in conjunction with $\Gamma^0_{MCC} = 8 \times 10^{-4}$ a.u., which was suggested by a few direct Γ_{MCC} calculations using the method of Díez Muiño et al. [31]. Accordingly, we used the Coster-Kronig transition rates $\Gamma_{LLC}(l, n) = (3 - l)\Gamma^0_{LLC} n^{\beta}$ with $\Gamma^0_{LLC} = 7 \times 10^{-3}$ a.u. It is noted that the rates for Coster-Kronig transitions are about an order of magnitude larger than the related Auger data [34].

It remains to consider transitions involving higher shells such as *KLM* and *KMC*. The rates for *KLM* and *KMM* were determined using the same scaling rules as in Eq. (4), however, the rates per spin state were assumed to be a factor of, respectively, 4 and 50 smaller than those for the *KLL* transitions. These factors are consistent with the scaling rules given previously [7]. Finally, the rates for transitions such as *KC*, *KLC*, *LMC*, etc. involving the *C* shell were scaled on the basis of calculations performed as in the work by Díez Muiño et al. [31]. It should be noted that the rates for transitions involving higher orbitals are not so critical for the present analysis.

Apart from the data for Auger and x-ray transitions, the cascade model needs rates for collisional

electron capture. We distinguish two types of electron capture processes. First, the upper orbitals such as the C shell receive electrons from the conduction band. As mentioned, this resonant capture is well described within the over-the-barrier model [7], which predicts a considerable flux of electrons when the higher orbital touches the surface. Hence, we used the following expression for the ingoing flux rate from Eq. (1)

$$\Gamma_C^{\text{in}}(\kappa, q_C) = \bar{q}_C \Gamma_{\text{pl}}^0 \begin{cases} e^{z/z_C} + f_0 e^{z/z_0} & \text{for } z < 0 \\ 1 & \text{for } z \geq 0 \end{cases} \tag{6}$$

where $\bar{q}_C = 17 - l - m - q_C$ is a statistical factor describing the missing charge in the C shell. The constant rate Γ_{pl}^0 that governs the formation of the C orbital, is attributed to the plasmon frequency of the jellium [30].

In Eq. (6) the distance z is measured from the jellium edge. Above the surface ($z < 0$) an exponential dependence is adopted, whereas inside the solid ($z \geq 0$) the rate is assumed to be constant. For $z < 0$ the two exponential terms correspond to side-feeding effects and contributions of Auger cascades from higher levels, respectively. Hence, the first exponential function governs the direct transfer of electrons from the conduction band into the C (or N) shell. Similar exponential dependencies have previously been adopted [27,28]. We have chosen $z_C = 1$ a.u. in accordance with the estimated size of the N shell. The second exponential function describes Auger transitions from higher lying orbitals which have previously collected charge via the over-the-barrier mechanism. To fit the experimental results for low-energy projectiles treated below, we have set $z_0 = 5$ a.u. in conjunction with $f_0 = 5 \times 10^{-3}$. The small value of the fraction f_0 indicates that the contribution from the Auger cascades in higher shell is minor. This finding is consistent with conclusion previously drawn from the over-the-barrier model by Burgdörfer et al. [7]. However, it should be emphasized that despite of the small f_0 value, the Auger cascades are essential for the spectra taken at very low projectile energies.

Second, we consider the electron transfer between localized inner orbitals occurring in binary collisions between the projectiles and target atoms. Such electron capture is assumed to take place into the M shell of the hollow projectile. Previously, an a priori method was given to treat these processes of charge exchange into hollow Ne atoms moving inside Al [16]. Molecular orbitals were evaluated [36] and the Landau-Zener model was utilized to determine related cross sections for electron capture. In the present work, we did not repeat this elaborate a priori procedure for Ar. A preliminary analysis showed that the molecular orbitals correlating with the Ar M and Si L shells in the Ar + Si system are similar to those considered for Ne + Al [16]. Hence, for the rates of electron capture into the Ar M shell we adopted essentially the previous results for the transition rates inside the solid. Moreover, above the surface, we assumed a distance dependence as in Eq. (6) using only the first exponential function where z_C was replaced by z_M representing a measure of the M shell radius. Finally, it is pointed out that charge exchange into the Ar L shell was disregarded as this process has been shown to be small [36].

It should be realized that the resonant charge exchange into the C shell is independent of the projectile velocity within the solid. This is contrary to the capture into the M shell which implies a strong velocity dependence of the transition rates. The previous studies of the Ne + Al system have shown that electron capture into hollow Ne exhibits a threshold-like energy dependence of the cross section [16,21]. Scaling these results by means of the projectile velocity, the corresponding capture rates for hollow Ar atoms increase strongly up to a few kiloelectron volts, whereas at higher energies the cross sections rise linearly with the projectile velocity. More details may be found in previous studies concerning electron capture into hollow Ne atoms [16,21].

After the determination of the model parameters and functions, the system of differential equations could be evaluated. Eqs. (1) and (2) were solved using an iterative procedure. First, Eq. (1) was evaluated for the full set of given configurations $\kappa = (l, m)$, where $m \leq 17 - l$ and $l \leq 8$, yielding the charge-state functions $q_C(\kappa, t)$. Then, Eq. (2) was solved in

ascending order of the $\kappa = (l, m)$ configurations by increasing m prior to l. This specific type of ascending order provides all solutions $N_\kappa(t)$ necessary for the next step of the iteration. A computer program was written to solve the differential equations (1) and (2). A typical run for a given projectile energy involves about 400 equations which could be solved numerically within about 15 min on a Pentium PC to obtain a complete set of functions $q_C(\kappa, t)$ and $N_\kappa(t)$.

4. Comparison with experiment

To compare the present model with experimental results, the functions $N_\kappa(t)$ are multiplied with the transition rates attributed to the measured process. For instance, the KL x-ray intensity, i.e. the number of photons ejected per unit time into the 4π solid angle, is given by

$$I_{KL}(t) = \Gamma_{KL}(\kappa)\, N_\kappa(t) \tag{7}$$

After time integration, one obtains the emission yield for KL x rays specified by the configuration κ

$$Y_{KL}(\kappa) = \int_{-\infty}^{\infty} \Gamma_{KL}(\kappa)\, N_\kappa(t)\, dt \tag{8}$$

which can be compared with the corresponding spectral intensities obtained in the experiment. Since the rate $\Gamma_{KL}(\kappa)$ is not dependent on time, it may be placed outside the integral. This is not necessarily possible when transitions from the C shell are considered.

To compare the present model with experiment we have chosen the high resolution x-ray spectra by Briand et al. [18]. The left column of Fig. 5 shows data for Ar^{17+} incident on SiH with the energies of 17 eV, 3.4 keV, and 170 keV. The spectra are composed of distinct peaks, each of which can be attributed to a specific number of l electrons occupying the L shell during x-ray emission. It is seen that the spectra change significantly as the projectile energy varies. At the lowest energy of 17 eV the spectrum consists of only a few prominent lines which are primarily due to the smallest L-shell occupation numbers $l = 1$ and 2.

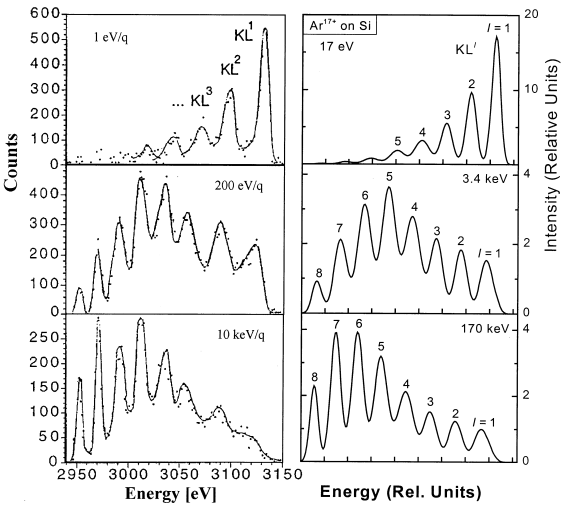

Fig. 5. Experimental K x-ray spectra [18] produced by Ar^{17+} at normal incidence on SiH for energies of 17 eV, 3.4 keV, 170 keV (left column), in comparison with theoretical results obtained using the present cascade model (right column). The peaks are attributed to the number l of electrons occupying the L shell during the x-ray transition. For a given l value a peak shift is observed due to a variation of the number m of M-shell electrons. The experimental yields are plotted in relative units whereas the theoretical yields are given in terms of the total number of x-rays ejected per incident ion.

Hence, at low projectile energies the L shell is barely occupied during K x-ray emission. At higher energies of 3.4 keV the spectrum exhibits intermediate occupation numbers for the L shell. Finally, when changing to the high energy of 170 keV the spectrum is still significantly altered. For instance, the $l = 8$ peak increases in intensity by a factor of $\sim$3 when the projectile energy is increased from 3.4 to 170 keV.

The right column in Fig. 5 shows the present model results for the emission yield $Y_{KL}(\kappa)$ from Eq. (8). In the present comparison we neglect possible effects arising from the fact that the Si surface used in the experiment is hydrogen terminated. For the lowest energy of 17 eV the incident ions are assumed to be accelerated by 80 eV due to image charge effects [13,37]. It is recalled that the emission yield is evaluated for a given configuration $\kappa = (l, m)$ denoting the occupation of the L and M shells. From Fig. 5 it is seen that the intensities of the theoretical line spectra compare well with the corresponding experimental data. In particular, the significant

Table 1
Mean number $\bar{m}$ of electrons in the M shell during K-X-ray emission for different projectile energies. The parameter l denotes the numbers of L shell electrons

Energy/l	1	2	3	4	5	6	7	8
17 eV	1.2	1.7	2.2	2.6	3	—	—	—
3.4 keV	5.1	6.3	6.8	7.0	7.2	7.4	7.6	7.6
170 keV	7.1	8.3	9.1	9.6	10	10	9.7	8.8

changes of the spectral structures with the projectile energy are well reproduced. This provides confidence that the present model accounts for the essential features of hollow Ar atoms interacting with a surface.

Close inspection of the experimental spectra shows that each peak is slightly shifted in energy as the projectile energy varies. This is due to the fact that the occupation of the M shell varies with varying projectile energy [6]. Thus, the centroid energy of the x-ray peaks provide information about the average number of electrons occupying the M shell during x-ray emission. The variation of the M-shell occupation is taken into account in the theoretical results. Each calculated peak for a given number of l electrons represents a superposition of Gaussian lines attributed to the different m values. Thus, the centroid energy of the theoretical peaks is determined by the mean number $\bar{m}$ of M-shell electrons and the width is governed by the corresponding m distribution. Table 1 shows results for $\bar{m}$ as a function of l which are found to be consistent with the peak position of the experimental spectra.

In Fig. 5 the striking feature is the strong energy dependence of the spectral structures. To explain the apparent change of the line intensities, Briand et al. [18] suggested that at low energies, such as 17 eV, the observed x rays originate from above-surface emission and at 3.4 keV and higher energies the emission below the surface dominates. It was argued that below the surface the N and M shells are rapidly filled giving rise to fast LMM Auger transitions so that the L shell is occupied by several electrons during the observation of the K x rays. Within this scenario, however, the velocity dependence of the charge transfer processes was neglected. In the following the attempt is made to verify the proposed scenario using the present model.

First, to study the role of the collisional charge transfer into the M shell we performed auxiliary calculations under the assumption that this charge transfer does not exist. The spectra for 17 eV and 3.4 keV calculated with negligible charge transfer remain unaltered with respect to those shown in Fig. 5. This can be explained by the fact that the electron capture processes are still small at these low energies. (Recall that the charge exchange cross sections exhibit a threshold at a few kiloelectron volts.) However, the newly calculated spectrum for 170 keV differs noticeably from the old one, in fact, it looks like that for 3.4 keV. This provides evidence that the differences between the previous spectra for 3.4 and 170 keV (Fig. 5) originate from electron capture into the M shell. The electron transfer processes may be visualized using the configuration matrix in Fig. 3. These processes move the system faster from the front to the back where, in turn, the progression from the left to the right is enhanced [note in Eq. (5) the strong m dependence of Γ_{LMM}]. Accordingly, relatively large intensities are observed for high l values in the 170 keV spectrum (Fig. 5).

Second, to verify the scenario of above- and below-surface emission we calculated the time-dependent K x-ray intensities by means of Eq. (7). Time can readily be transformed to a length for projectiles moving on a straight line with a constant velocity. The results for different l values are given in Fig. 6 as a function of the distance z from the jellium edge. The graphs refer to the same energies chosen before in Fig. 5. The plotted intensities provide clear evidence that for the lowest energy of 17 eV all x rays are ejected above the surface. On the other hand, the data for 3.4 keV and higher energies indicate that the major part of the K x rays is ejected below the surface. Hence, our quantitative analysis confirms an essential part of the scenario suggested by Briand et al. [18]. Moreover, from Fig. 6 it is seen that the x rays attributed to the lowest numbers $l = 1$ and 2 are ejected first, i.e. the x-ray emission is time ordered with respect to an increase of the occupation number l. Similar phe-

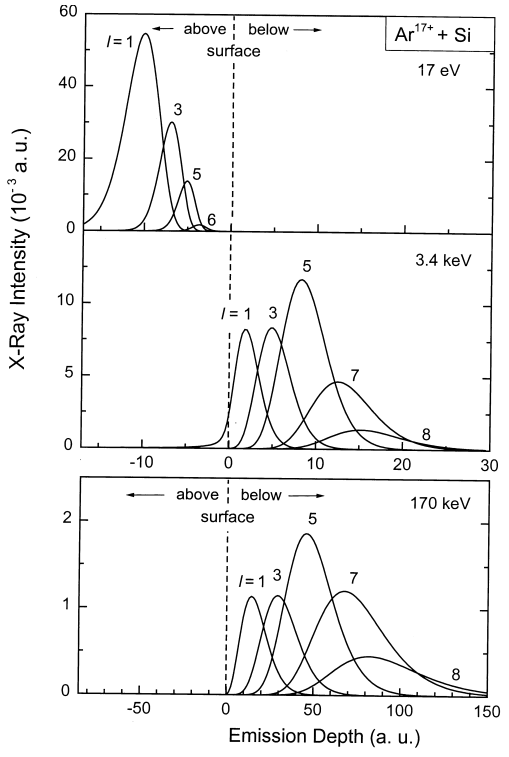

Fig. 6. Intensity of *K* x rays, i.e. the total number of photons per ion and unit length, from Ar^{17+} incident at a Si surface at the energies 17 eV, 3.4 keV, 170 keV. The data are plotted as a function of the distance measured from the jellium edge of the surface. Negative and positive distances refer to above- and below-surface emission, respectively. Individual curves are labeled with the number *l* of electrons occupying the *L* shell during x-ray emission.

nomena have earlier been observed in Auger electron spectra for which the lowest *l* component was assumed to be due to above-surface emission, whereas the remainder of the spectrum was attributed to the emission from the bulk [38,39].

From the present results for the x-ray intensities, the filling time of the hollow atoms can be estimated. For instance, at the energy of 3.4 keV the x-ray emission takes place along a distance of about 30 a.u. (Fig. 6) which corresponds to an emission within a time interval of about 500 a.u. This interval decreases somewhat when projectiles of higher energies are used. This is due to the fact that in the latter case the charge exchange processes gain importance. Hence, the typical filling time, corresponding to the lifetime of the hollow atoms, is of the order of a few 10^{-14} s. This time is much longer than a few 10^{-17} s which is the time unit for atomic processes.

5. Conclusions

The present analysis shows that the modeling of hollow Ar atoms is a highly challenging task. To keep this task manageable we have combined two methods of treating the numerous configurations produced during the cascading decay of a hollow atom. Individual configurations were considered for the *K*, *L*, and *M* shells, whereas a mean charge was assumed for the *C* shell representing the higher shells. Nevertheless, the present analysis involves the solution of several hundred rate equations to obtain the occupation numbers for the individual configurations.

The consideration of a time-dependent charge in the *C* shell goes beyond previous studies of hollow Ne atoms [16,17]. In the latter work, the *C* shell was assumed to be rapidly filled to the maximum charge, whereas in the present model a charge cloud is dynamically produced above the surface and possibly in a shallow region below the surface. The new treatment of above-surface phenomena is found to be essential for very slow projectiles, whereas the previous analysis is expected to be valid for ions with energies above a few kiloelectron volts. For instance, the emission of *K* x rays from 17 eV projectiles are shown to occur exclusively above the surface. Also, the model calculations shows quantitatively that x-ray emission is time ordered with respect to the rising occupation of the *L* shell. Such effects have been considered in several studies [18,38,39]. Moreover, at energies larger than 3.4 keV the x-ray emission takes place essentially below the surface. These findings confirm the interpretation in the previous x-ray work [18]. However, contrary to the previous interpretations, we attribute essential features in the spectra to velocity-dependent charge capture into the hollow Ar atom.

The present model should by no means be considered as complete. Further work is needed to improve the determination of the various rates and scaling rules used in this analysis. In particular, more work is required to refine the treatment of above-surface

phenomena. The parameters used in this treatment, such as the filling rate of the C shell and the energy due to image charge acceleration should be verified in detail. For the future, it would be useful to study Auger electron emission produced by Ar^{17+} impact on a surface. In particular, the absolute yields of the ejected electrons could provide a sensitive tool to verify the present cascade model.

Acknowledgements

The authors are indebted to Professor Andres Arnau, Dr. Martin Grether, Professor Jean-Pierre Briand, Dr. Brigitte Ban d'Etat, Professor Reinhold Schuch, and Dr. John D. Gillaspy for enlightening communications concerning various aspects of this work. Helpful comments on the manuscript by Professor John Tanis are gratefully acknowledged.

References

[1] A. Arnau, F. Aumayr, P.M. Echenique, M. Grether, W. Heiland, J. Limburg, R. Morgenstern, P. Roncin, S. Schippers, R. Schuch, N. Stolterfoht, P. Varga, T.J.M. Zouros, HP. Winter, Surf. Sci. Rep. 27 (1997) 117.
[2] H.D. Hagstrum, Phys. Rev. 91, 543 (1953); 96 (1954) 325.
[3] U.A. Arifov, E.S. Mukhamadiev, E.S. Parilis, A.S. Pasyuk, Zh. Tekh. Fiz. 43 (1973) 375 [Sov. Phys.-Tech. Phys. 18 (1973) 240].
[4] M. Delaunay, M. Fehringer, R. Geller, P. Varga, HP. Winter, Europhys. Lett. 4 (1987) 377.
[5] H.J. Andrä, Nucl. Instrum. Methods Phys. Res. B 43 (1989) 306.
[6] J.-P. Briand, L. de Billy, P. Charles, S. Essabaa, P. Briand, R. Geller, J.P. Desclaux, S. Bliman, C. Ristory, Phys. Rev. Lett. 65 (1990) 159.
[7] J. Burgdörfer, P. Lerner, F.W. Meyer, Phys. Rev. A 44 (1991) 5674.
[8] L. Folkerts, R. Morgenstern, Europhys. Lett. 13 (1990) 377; L. Folkerts, R. Morgenstern, Z. Phys. D 21 (1991) S351.
[9] F.W. Meyer, S.H. Overbury, C.C. Havener, P.A. Zeijlmans van Emmichoven, D.M. Zehner, Phys. Rev. Lett. 67 (1991) 723.
[10] R. Köhrbrück, K. Sommer, J.P. Biersack, J. Bleck-Neuhaus, S. Schippers, P. Roncin, D. Lecler, F. Fremont, N. Stolterfoht, Phys. Rev. A 45 (1992) 4653.
[11] S. Schippers, S. Hustedt, W. Heiland, R. Köhrbrück, J. Kemmler, D. Lecler, J. Bleck-Neuhaus, N. Stolterfoht, Phys. Rev. A 46 (1992) 4003.
[12] J. Burgdörfer, Review of Fundamental Processes and Applications of Atoms and Ions, C.D. Lin (Ed.), World Scientific, Singapore, 1993, p. 517.
[13] F. Aumayr, HP. Winter, Comments At. Mol. Phys. 29 (1994) 275.
[14] J. Burgdörfer, C. Reinhold, F. Meyer, Nucl. Instrum. Methods Phys. Res. B 98 (1995) 415.
[15] A. Arnau, R. Köhrbrück, M. Grether, A. Spieler, N. Stolterfoht, Phys. Rev. A 51 (1995) R3399.
[16] N. Stolterfoht, A. Arnau, M. Grether, R. Köhrbrück, A. Spieler, R. Page, A. Saal, J. Thomaschewski, J. Bleck-Neuhaus, Phys. Rev. A 52 (1995) 445.
[17] N. Stolterfoht, D. Niemann, M. Grether, A. Spieler, C. Lemell, F. Aumayr, HP. Winter, Nucl. Instrum. Methods Phys. Res. 124 (1997) 303.
[18] J.-P. Briand, G. Giardino, G. Borsoni, M. Froment, M. Eddrief, C. Sébenne, S. Bardin, D. Schneider, J. Jin, H. Khemliche, Z. Xie, M. Prior, Phys. Rev. A 54 (1996) 4136.
[19] J.-P. Briand, S. Thuriez, G. Giardino, G. Borsoni, M. Froment, M. Eddrief, C. Sébenne, Phys. Rev. Lett. 77 (1996) 1452.
[20] J.-P. Briand, S. Thuriez, G. Giardino, G. Borsoni, Le Roux, M. Froment, M. Eddrief, C. de Villeneuve, B. D'Etat-Ban, C. Sébenne, Phys. Rev. 55 (1997) 1.
[21] M. Grether, D. Niemann, A. Spieler, N. Stolterfoht, Phys. Rev. A 56 (1997) 3794.
[22] R. Page, A. Saal, J. Thomaschewski, L. Aberle, J. Bleck-Neuhaus, R. Köhrbrück, M. Grether, A. Spieler, N. Stolterfoht, Phys. Rev. A 52 (1995) 1344.
[23] H. Limburg, S. Schippers, I. Hughes, R. Hoekstra, R. Morgenstern, S. Hustedt, N. Hatke, W. Heiland, Phys. Rev. A 51 (1995) 3873.
[24] J. Thomaschewski, J. Bleck-Neuhaus, M. Grether, A. Spieler, N. Stolterfoht, Phys. Rev. A 57 (1998) 3665.
[25] J. Ducrée, F. Casali, U. Thumm, Phys. Rev. A 57 (1998) 338.
[26] J. Ducrée, J. Mrogenda, E. Reckels, M. Rüther, A. Heinen, Ch. Vitt, M. Venier, J. Leuker, H.J. Andrä, R. Díez Muiño, Phys. Rev. A 57 (1998) 1925.
[27] S. Wimecki, C.L. Cocke, D. Fry, M.P. Stöckli, Phys. Rev. A 53 (1996) 4228.
[28] W. Huang, H. Lebius, R. Schuch, M. Grether, N. Stolterfoht, Phys. Rev. A 56 (1997) 3777; W. Huang, H. Lebius, R. Schuch, M. Grether, A. Spieler, N. Stolterfoht, Nucl. Instrum. Methods Phys. Res. B 135 (1998) 336.
[29] E. Zaremba, L.M. Sander, H.B. Shore, J.H. Rose, J. Phys. F 7 (1977) 1763.
[30] D. Pines, Elementary Excitations in Solids, Benjamin, New York, 1964.
[31] R. Díez Muiño, A. Salin, N. Stolterfoht, A. Arnau, P.M. Echenique, Phys. Rev. A 57 (1998) 1126.
[32] C.P. Bhalla, Phys. Rev. A 8 (1973) 2877.
[33] E.J. McGuire, Phys. Rev. A 3 (1971) 587.
[34] M.O. Krause, J. Phys. Chem. Ref. Data 8 (1979) 307.
[35] F.P. Larkins, J. Phys. B 9 (1971) L29.
[36] N. Stolterfoht, in Progress in Atomic Spectroscopy, Part D, H. Kleinpoppen (Ed.), Plenum, New York, 1987, p. 415.
[37] C. Auth, T. Hecht, T. Igel, H. Winter, Phys. Rev. Lett. 74 (1997) R2523.
[38] J. Das, R. Morgenstern, Phys. Rev. 47 (1993) R755.
[39] H.J. Andrä, A. Simionovici, T. Lamy, A. Brenac, A. Pesnelle, Europhys. Lett. 23 (1993) 361.